Accepted manuscript doi:
10.1680/jstbu.17.00172

Submitted: 02 November 2017

Published online in 'accepted manuscript' format: 24 May 2018

Manuscript title: Effect of Geometrical Properties on the Strength of Externally Prestressed Steel-Concrete Composite beams

Authors: Anwar Badawy Abu-Sena[1], Ibrahim Galal Shaaban[2], Mohamed Salah El-din Soliman[3] and Khaled Abd-Allah Mohamed Gharib[1]

Affiliations: [1]Faculty of Eng. (Shoubra), Benha University, Egypt; [2]University of Liverpool (On Sabbatical, Benha University, Egypt); [3]San Jose State University, USA

Corresponding author: Ibrahim Galal Shaaban, University of Liverpool (On Sabbatical, Benha University, Egypt). Tel.: +447403567773; Fax: 07403567773.

E-mail: ibrahim.shaaban@liverpool.ac.uk

Accepted manuscript doi:
10.1680/jstbu.17.00172

Abstract

A parametric study was carried out to investigate the structural behavior of composite steel-concrete T-beams under different prestressing conditions. The studied parameters include different cases of loading, tendon profiles, beam spans, initial prestressing levels and different dimensions of steel sections and concrete deck. The studied beams were modeled by the finite element software ANSYS. The effect of three geometrical parameters was investigated for three different tendon profiles. It was found that straight tendon profiles are more appropriate for beams under distributed loads, while draped tendon profile is more convenient for beams under concentrated loads. In addition, the ratio of the tension flange area to the compression flange area is the most effective geometrical parameter on the ultimate resistance of the studied prestressed beams. For instance, increasing this ratio from 1 to 3 resulted in increasing the additional resistance of the beam due to prestressing from 15.4% to 46.1%. For composite beams, the presence of the concrete slab prevented the lateral-torsional buckling and accordingly minimized the effect of the span. Moreover, increasing the slab thickness to width ratio resulted in enhancing the average increase in beam strength from 13.5% to 19.9%.

Keywords: Beams and girders; Cables and tendons; Composite structures; Steel structures; Finite element modeling; External prestressing; Geometrical properties

Accepted manuscript doi:
10.1680/jstbu.17.00172

1. Introduction

Two types of structures have intensively been adopted for the construction of bridges during the past few decades; namely the prestressed concrete beams and the composite steel beams. External prestressing of composite beams is mainly employed in bridge engineering and mostly to strengthen or rehabilitates of existing structures. Such advantages are generally attracting researchers to further study and enhance understanding the performance of this type of bridge construction. Combining the major benefits for both of the aforementioned structures has attracted the attention of the designers of bridge systems to use prestressed composite steel bridge in recent years. Externally prestressed steel-concrete composite members have been used since the late 1950s in buildings and bridge construction. In addition, external post-tensioning has been extensively applied in existing bridges to strengthen structures or to increase the ultimate capacity to accommodate heavier loads. Composite steel–concrete beams prestressed with external tendons offer several major advantages; e.g., elastic behavior under heavier loads, increased ultimate capacity, improved fatigue and fracture behavior [1]. Lorenc and Kubica [1] studied the behavior of composite beams prestressed with external tendons experimentally. It was concluded that in order to properly determine the load carrying capacity of a composite beam prestressed by external tendons, the correct value of the force in the tendons in the ultimate state must be assumed. Chen and Gu [2] investigated the ultimate load carrying capacity of composite beams prestressed with external tendons under positive moment. It was observed that adding prestressing by external tendons to the composite beams may significantly increases the yield load and the ultimate resistance of these beams. Dall'Asta, et al [3] conducted a research on a simplified method for failure analysis of concrete beams prestressed with external tendons. They concluded that the flexural strength of externally prestressed beams could not be evaluated by a local analysis of the critical sections.

Experimental and analytical studies were carried out to investigate the behavior of simply supported prestressed steel-concrete composite beams by Nie et al [4]. They proposed a reduced stiffness method for calculating the deflection overstressed composite beams. Zona, et al [5] studied a simplified method for the analysis of externally prestressed steel-concrete composite beams. They introduced a simplified method for evaluating the tendon traction increment at collapse and consequently the beam flexural strength without requiring a nonlinear analysis of the whole beam-tendon structural system. Behavior of prestressed concrete bridge girders was studied by Angomas [6]. He concluded that the AASHTO LRFD 2004 [7] refined method is reasonably accurate in predicting the prestressing losses. A finite element model for composite beams prestressed by external slipping tendons was presented by Dall'Asta and Zona [8]. The proposed formulation involves composite beams with deformable shear connection. The authors stated that the proposed approach could be implemented in existing nonlinear finite element programs with no additional iterative procedures. Choi et al [9] studied external post-tensioning of composite bridges by a rating equation considering the increment of a tendon force due to live loads. They illustrated a systematic procedure of external post-tensioning technique for strengthening or rehabilitation of steel-concrete

Accepted manuscript doi:
10.1680/jstbu.17.00172

composite bridges. Dabaon et al [10] investigated ultimate behavior of externally prestressed composite beams with partial shear connection. Authors presented 3D and uniaxial finite element models to describe the long-term behavior of such beams. Based on reported results, authors concluded that the long-term factors have significant effect on behavior of beams. They concluded also that relaxation of tendon had the major effect among other factors.

El-Zohairy and Salim [11] implemented a parametric study for post-tensioned composite beams with external tendons. The results demonstrated that at the same tendon eccentricity, the trapezoidal profile shows better behavior for the strengthened beams. However, more ductility is obtained when using the straight tendon profile. Chandramohanmouli and Kumar [12] carried out a nonlinear finite-element analysis to investigate the behavior up to failure of simply supported composite steel-concrete beams with external prestressing. The analytical tests carried out for the different studied cases indicated that the load-deflection behavior and the ultimate loads are in good agreement with the published experimental results. Ibrahim et al [13] investigated the effect of several important parameters on the behavior of external prestressed composite steel-concrete beams by conducting a parametric study. The finite element results for simply supported beams with full shear interactions showed stiffer behavior compared to beams with partial shear interactions. Liban and Tayşi [14] examined the behavior up to failure of cantilever composite steel-concrete beams which are prestressed externally. The authors concluded that adding prestressed tendons to composite beams significantly increased the yield load and the ultimate load. They concluded also that the farther the tendons are located from the neutral axis, the greater is the increase in strength. Ibrahim and Salman [15] investigated analytical continuous composite steel-concrete beam with external prestressing by conducting a parametric study. It was found that as the compressive strength of concrete and the effective prestressing stress increased the ultimate load capacity increased.

Lou and Xiang [16] described a numerical analysis procedure of second-order effects of externally prestressed concrete beams. The authors revealed that the second-order effects are the most important characteristics which distinguish an external tendon system from an internal un-bonded one. This study lead to a conclusion that the provision of one deviator at the section of the maximum beam deflection can effectively minimize the second-order effects for simply-supported prestressed concrete beams with external straight horizontal tendons even for a very slender beam. Ibrahim et al [17] implemented a parametric study of composite steel-concrete beams with external prestressing to investigate the factors affecting their behavior. It was found from the numerical analysis that the predicted ultimate loads are increased by increasing compressive strength of concrete, effective prestressing stress, the ratio of the depth to width of concrete slab, shear interactions, or ratio of top flange area to bottom flange area. It was also found that stiffeners web plate has no significantly effect on the behavior of prestressed composite steel-concrete beams. Bukka R. S. et al [18] conducted a study on non-linear analysis of composite beam slab junction with shear connectors using ANSYS 14 [19]. They stated that composite action depends on the interaction between the reinforced concrete slab, the steel profile, and the shear connection. Therefore, a perfect

composite action cannot be obtained in practice due to deformability of the shear connectors. The behavior of steel box girders prestressed with external tendons was studied by Mahgoub et al [20]. A finite-element model for the flexural behavior of a simply supported steel girder with a box-shaped cross-section and prestressed by external tendons was established. Box girders with and without prestressing were tested to evaluate the effectiveness of the technique. It was concluded that prestressing improves the flexural capacity of a girder and its effect is proportional to the size of the applied external load.

Shiming et al [32] investigated the inelastic buckling of steel-concrete composite beams prestressed with external tendons. A parametrical analysis was carried out to predict load carrying performance and buckling moment resistance of prestressed composite beams. The computed buckling moment ratios were compared with the Chinese Codified steel column design curve. The authors concluded that the tentative design method based on this curve could be used in assessment of buckling strength of composite beams in a term of the modified slenderness proposed by the authors. Numerical modeling of externally prestressed steel-concrete composite beams was carried out by Tiejiong et al [33]. Geometric and material nonlinearities were considered as well as time-dependent effects. Authors validated the proposed model by comparisons with available experimental data. Typical short and long-term responses of steel–concrete composite beams with and without external prestressing were evaluated.

2. Aim of the Study

The current theoretical investigation aims to study the ultimate strength of externally prestressed composite steel-concrete T-beams under different geometrical parameters. This study includes different cases of loading, tendon profiles, beam spans, initial prestressing levels, and different dimensions of steel sections and concrete deck thickness. The finite element analysis was carried out using the computer program ANSYS 14.0 [19]. The results were firstly verified by the experimental results available in the literature and then an extensive study for the different geometrical parameters involved modeling 2160 studied beams was carried out to assess the effect of the geometrical parameters on the behavior of composite T-beams.

3. Finite Element Modeling of the Studied Beams

ANSYS program of version 14.0 [19] was used for analyzing the externally prestressed composite beams. Three-dimensional brick element with 8 nodes from ANSYS element library was used to model the concrete slab (SOLID65). The most important aspect of this element is the treatment of nonlinear material properties. Three-dimensional 4-node shell element (SHELL181) was used to represent the steel beam flanges and webs. (SHELL181) is well suited to model linear, warped; moderately-thick shell structures. (LINK180) element is a uniaxial tension-compression element with three degrees of freedom at each node. It was used to represent the external cable and reinforcement bars. The initial prestressing on tendon was applied as initial strain in link elements which presents the prestressing tendons. Reduction in

Accepted manuscript doi:
10.1680/jstbu.17.00172

prestressing stress was noted as the initial strain was applied immediately at first load step and made the beam cambered. So that, the initial strain was increased to overcome that reduction in stress to assure that targeted initial prestressing level is achieved. The frame element (BEAM188), which is a uniaxial element with tension, compression, torsion, and bending capabilities, was used to model shear connectors. Each shear connector is presented by four frame elements, one element between top of upper steel flange and bottom of concrete slab, and three elements in the concrete slab. Bond between steel section and concrete deck of composite section is very weak compared with junction due to shear connectors, and therefore, it was neglected in modeling composite action. In order to overcome large displacement effects, all aforementioned elements have large deflection and large strain capabilities.

Beams in the present study are simply supported and the supports were modeled as hinges and roller supports exist at ends. The hinge support was modeled by constraining nodes in the vertical and longitudinal direction ((Uy, Uz) = 0), as shown in Figure 1 (a).To model the roller support, nodes of the end line at the bottom flange were constrained in the vertical direction (Uy = 0) as shown in Figure 1 (b). All nodes at hinged and roller supports were also constrained in horizontal direction (Ux = 0) for stability purposes. Uniformly distributed loads were applied on middle line of nodes on the top surface of concrete slab. Concentration of stress in the concrete slab at the point of concentrated loads is prevented by using a small bearing plate placed between the concentrated loads and the concrete slab. Failure in the finite element modeling is usually accompanied with increasing iterative displacements and a continuous growth in the dissipated energy. Hence, the convergence of the iterative process cannot be achieved, and a massage is given by the software to indicate that beam failure is achieved.

4. Modeling of Material Properties

In order to obtain an accurate modeling of the studied composite steel-concrete beams, choosing appropriate material modeling for concrete and steel is essential. This could be achieved by utilizing the plasticity model for stress-strain relation of concrete under compressive stresses based on work done by Desayi and Krishnan [21]; as shown in Figure 2 (a). Multi-linear curve was used to help with convergence of the nonlinear solution algorithm. Concrete subjected to tensile stresses was allowed to crack because minor tensile stresses were expected for concrete slab on top of simply supported composite beam. While the stress-strain diagram of steel under either tensile stresses or compressive stresses, for simplicity, was assumed to be two straight lines: the first line starts from the origin with a slope equals to (E_s) up to (f_y), and the second line was horizontal. However, for practical software applications the second line is assumed to have a very small slope. Therefore, the bilinear stress-strain relationship indicated in Figure 2 (b) was adopted. The strain hardening modulus (E_t) is assumed to be (0.03 E_s) to avoid convergence problems during iteration [22].

5. Verification of Finite Element Analysis

Accepted manuscript doi:
10.1680/jstbu.17.00172

The aim of this section is to verify the ANSYS results of the nonlinear finite element model developed to investigate the behavior and strength of prestressed composite steel-concrete beams. The verification study is established to prove that both the adopted idealization and elements are adequate to accurately predict the failure loads, deformed shape, and load-displacement relations compared to the experimental results by other researchers in literature. For this purpose, results obtained from ANSYS finite element analysis are compared to the corresponding values obtained by previous experimental researches. There is many reports that presents experimental work on externally prestressed composite beams [23-29]. In this section only two reports are considered for verification. Hence, two various types of prestressed composite steel- concrete beams with available experimental results have been analyzed. Material properties of the two verification sample beams are summarized in Table 1 for components of composite beams including steel beam, concrete slab, and prestressing tendon. Typical cross-section of externally prestressed composite beam is shown in Figure 3. Geometrical properties of verification sample beams are presented in Table 2.

5.1 The First verification beam (VB1)

Saadatmanesh et al [30] tested a simply supported composite steel-concrete beam prestressed with high-strength steel tendon and subjected to two concentrated loads, as shown in Figure 4 (a). The steel beam is prestressed with two 16mmdiametertendonrunning the full beam length 57 mm below the bottom (tension) flange. The experimental and finite element model load-deflection curves are shown in Figure 4 (b). Good agreement was obtained between the experimental load-deflection curve and the predicted finite element curve throughout the entire loading range of the tested beam. It can be seen from Figure 4 (b) that the computed ultimate load is very close to the experimental ultimate load. The predicted ultimate load level (64.14t)was detected quite well compared with that experimentally observed (64.1t).The deformed shape for camber arising from the effect of prestressing force in the external tendon is shown in Figure 4 (c), while the deformed shape due to externally applied loads at ultimate state is shown in Figure 4 (d).

5.2 The second verification beam (VB2)

Ayyub et al [31] tested three prestressed composite steel-concrete beams (A, B, and C) under positive bending moment. Beams (C) was selected as (VB2) for the current analysis. As shown in Figure 5(a), the beam (VB2) is prestressed with draped tendon profile. The tendons are anchored at both ends of the composite section, 32 mm below the top flange and were positioned between the loading points 30 mm above the bottom flange. The load-mid-span deflection curve of the prestressed composite steel-concrete beam (VB2) obtained from the finite element analysis was in a good agreement with corresponding experimental data as shown in Figure 5 (b). The ratio of the experimental ultimate load to the predicted one was 0.94. Camber due to effective prestressing in the first load step is shown in Figure 5 (c). The deflected shape due to external force applied at ultimate load is shown in Figure 5 (d).

Accepted manuscript doi:
10.1680/jstbu.17.00172

6. Parametric Study

After validating the analysis tool, a finite element study was conducted to determine the parameters which may affect the behavior and strength of prestressed composite beams. It is worth mentioning that limitations and recommendations specified by codes of practice were satisfied in the selected specimens. Table 3 presents the dimensions of steel sections. It can be observed from Table 3 that, web depth to thickness ratio and flange width to thickness ratio are selected to avoid local buckling according to design codes recommendations [22]. In this study beams of steel sections Group (A) and (B) are assigned to 8.00, 10.00, and 12.00 m spans, while deeper beams with steel sections Group (C) and (D) are assigned to 12.00, 14.00, and 16.00 m spans. The concrete deck connected to steel sections has a concrete deck thickness to width ratios, h_c /B_c, of 0.10, 0.12, and 0.145. The total concrete deck cross-sectional area was considered to be, 1000 cm^2, for the three (h_c /B_c) values in order to keep the concrete area constant. Width and thickness of concrete deck are selected in accordance with limits of design codes [22]. The varieties of steel sections and concrete deck dimensions with different spans provide 108 non-prestressed composite beams (NP). To produce prestressed composite beams, the studied beams were prestressed by two tendons and each of them has strands with150 mm^2 cross-sectional area. Tendons are anchored to 35 mm plates at ends and adjusted to its positions by 15 mm saddle plates. Tendons are not connected to saddle plats directly but through springs which allow for slippage between them. The initial prestressing applied on tendons induced three different stress levels of $0.4F_y$, $0.5F_y$, and $0.6F_y$, to satisfy the design codes' limitations.

Tendons are adjusted in three different profiles as shown in Figure 6. The first tendon profile (SA) consists of two straight tendons located 3 cm above bottom flange adjusted by four saddle plates as shown in Figure 6(a). The second tendon profile (SB) also consists of two straight tendons located 3 cm below bottom flange adjusted by four saddle plates as shown in Figure 6 (b). The third tendon profile (DR) was draped shape consists of two tendons as shown in Figure 6 (c). A typical cross-section of these beams is shown in Figure 3. The non-prestressed composite beams and the prestressed composite beams for the three tendon profiles were analyzed twice. Once under two concentrated loads 1.60 m apart and the other under uniformly distributed loads that produces a total number of 2160 beams. Table 4 summarizes the properties of materials of prestressed composite beams. Full composite action between steel sections and concrete slab was achieved by providing sufficient shear connectors.

7. Results and Discussion

Effect of previously mentioned parameters was investigated for each tendon profile for beams subjected to concentrated loads or distributed loads. For each parameter, the results of parametric study are presented generally and the results of the two main sections are discussed in detail.

7.1Effect of Steel Flanges Area Ratio

Accepted manuscript doi:
10.1680/jstbu.17.00172

It may be an advantage to use steel section having relatively larger bottom flange compared to the top flange. Therefore, the steel section flanges area ratio is an important parameter. The steel flanges area ratio is the result of dividing the area of the bottom flange A_{fb} (flange in tension) by the area of top flange A_{ft} (flange in compression). Variation of prestressed composite beams flexural capacities with the steel flanges area ratio will be presented for different tendon profiles hereafter in the next subsections and as shown in Figures 7-12.

7.1.1 Straight tendon profile above tension flange (SA)

Ultimate resistance values, Mu, of composite beams prestressed with first tendon profile (SA) were compared with ultimate resistance values, M_{uo}, of the corresponding non-prestressed composite beam with (A_{fb}/A_{ft} = 1.0). The percentage of increase in ultimate resistance due to prestressing was calculated. The maximum, minimum, and average percentage of increase in ultimate resistance is shown in Figures7 (a) and (b) for beams under concentrated and distributed loads. It can be observed that, the ultimate resistance of beams prestressed by straight tendon above the bottom flange increased by increasing the steel flange area ratio. It can be also noticed that the effect of prestressing of composite beams under distributed loads is more significant than prestressing beams under concentrated loads. This effect may be attributed to the tendon profile which has a straight profile above the bottom flange that produced prestressing moment with constant value along the beam length resisting the applied moment. The prestressing bending moment diagram is closer to the distributed load bending moment diagram rather than the bending moment of concentrated loads. Therefore, the effect of prestressing on beams under distributed loads is more significant than that for those under concentrated loads using straight tendon above bottom flange.

Figure 8 shows also the effect of changing steel flanges area ratio in the presence of prestressing force applied on composite beams. The initial prestressing force applied on the tendon was assumed to be (0.40 F_y) and the concrete deck thickness to width ratio was (h_c/B_c = 0.10). These values were considered standard for similar figures hereafter. Figures 8 (a) and 8 (b) presented the relation between ultimate moment ratio (M_u/M_{uo}) and steel flanges area ratio (A_{fb}/A_{ft}) for beams of steel section Group (A) subjected to concentrated and distributed loads, respectively. The ultimate moment of beams of steel section Group (B) is presented in Figures 8 (c) and (d) for beams under concentrated and distributed loads, respectively. It can be noticed that there is a direct relation between ultimate moment and steel flanges area ratio. The ultimate moment ratio increased by increasing steel flanges area ratio. The effect of prestressing is more significant on beams with (A_{fb}/A_{ft}) ratio less than two.

7.1.2 Straight tendon profile below tension flange (SB)

Beams prestressed by second tendon profile (SB) are investigated in this section. Figures 9 (a) and (b) presented the maximum, minimum, and average values of percentage of increase in

Accepted manuscript doi:
10.1680/jstbu.17.00172

resistance for beams subjected to concentrated and distributed loads respectively. It can be observed that increasing the steel flanges area ratio led to enhancing the ultimate resistance. This was noticed for the studied beams under concentrated and distributed loads. The Percentage of increase in resistance of beams under distributed loads is more significant than that for beams under concentrated loads. To thoroughly investigate the behavior, results were divided into groups and compared individually hereafter. Results of beams having steel section Group (A) are presented in Figures 10 (a) and (b). Results of prestressed composite beams of steel section Group (B) are presented in Figures 10 (c) and (d). Direct relationship between steel flanges area ratio and ultimate moment ratio was observed. The ultimate resistance increased by increasing steel flanges area ratio especially for (A_{fb}/A_{ft}) less than two.

7.1.3 Draped tendon profile (DR)

Beams prestressed by draped tendon profile are investigated in this section. The maximum, minimum, and average values of percentage of increase in resistance are presented in Figure 11.It can be observed that, the ultimate resistance of beams with draped tendon increased by increasing steel flange area ratio. In addition, it was noticed that the effect of prestressing of composite beams under distributed loads is larger than that for beams under concentrated loads with minor difference (less than 2%).To avoid the effect of other parameters affecting the resistance of beams, Figures 12 (a) and (b) presented the relation between ultimate moment ratio and steel flanges area ratio for beams of Group (A). Results of prestressed composite beams of Group (B) are presented in Figures 12 (c) and (d). As shown in these figures, increasing steel flanges area ratio led to a higher ultimate moment ratio.

It can be seen from Figures 7 to 12 that increasing the steel flange area ratio resulted in higher ultimate resistance. Increasing (A_{fb}/A_{ft}) ratio from 1 to 3 led to an average increase in ultimate moments of beams under concentrated loads from 15.4% to 41.6 % and an increase in the resistance of beams under distributed loads from 17.1% to 46.1%. This was in agreement with the work carried out by Ibrahim et al [12] where they found that the unsymmetrical I-section steel beam with wider bottom flange used in prestressed composite steel- concrete beam is more effective without change of total cross section area. They found also that the increase in ultimate load of beams subjected to four point loads (nearly distributed load) was greater than that in the beams subjected to a mid-span single load.

7.2 Effect of Beam Span (L)

The parametric study covers range of spans from 8.00 to 16.00 m. Effect of prestressing composite beams with different spans is studied. The studied beams are divided into groups according to prestressing tendon profile. Each prestressed composite beam is compared with the corresponding non-prestressed composite beam as will be discussed in the next subsections and as shown in Figures 13-20.

Accepted manuscript doi:
10.1680/jstbu.17.00172

7.2.1 Straight tendon profile above tension flange (SA)

Statistical data for prestressed composite beams subjected to concentrated and distributed loads is presented in Figures13, and 14 for beams of steel section depth of 500 and 750 mm respectively. These figures presented minimum, maximum, and average percentage increase in ultimate resistance of beams. It can be seen from the figures that the ultimate resistance tends to increase by increasing span with minor variation between different spans. Figure 15 shows the effect of changing beam span on the ultimate moment resistance of beams with steel sections (A1) and (B1). It can be seen from Figure 15that increasing the beam span led to enhancing the ultimate resistance of beams generally. However, the ultimate moment resistance of beams under distributed loads of Section (A1) were slightly affected by changing beam span as shown in Figure 15 (a) and the beams of Section (B1) under concentrated loads showed the same slight effect on the ultimate moment resistance by increasing span. Figure 16 (a) presents the ultimate resistance of beams having steel Sections (C1). The general trend of these beams is the reduction in ultimate resistance by increasing beam span. Figure 16 (b) shows that the increase in beam span led to enhancing the ultimate moment resistance for beams with steel section (D1).

7.2.2 Straight tendon profile below tension flange (SB)

Results of the parametric study of composite beams prestressed by straight tendon below the bottom flange are discussed hereafter. Figures 17 and 18 show the results of beams under concentrated and distributed loads, for depths of 500 and 750mm respectively. It can be seen from the figures that, generally, changing span has a minor effect on the percentage increase in the resistance. Figure 19 (a) shows the effect of changing beam span on the ultimate resistance for beams with Section (A1). It can be seen from the figure that the ultimate resistance of beams under concentrated loads increases by increasing beam span, but in the contradiction, it decreases for beams under distributed loads. It can be seen from Figure 19 (b) that the ultimate resistance of beams of Section (B1) under concentrated loads decreases by increasing beam span, while it increases by increasing beam span for beams under distributed loads. For beams of Sections (C1) and (D1), Figure 20 shows that the ultimate resistance varied with changing the beam span without a certain pattern.

7.2.3 Draped tendon profile (DR)

Figures 21 and 22 show comparison between ultimate resistance of beams under concentrated loads and distributed loads, for steel sections depth of 500 and 750 mm, respectively. Generally, the percentage of increase in the ultimate resistance reduced by increasing span with minor variation in resistance for different (h_c/B_c) ratios. Figures 23 (a) and (b) show the effect of changing beam span on the ultimate resistance of beams of Sections (A1) and (B1). No obvious trend could be observed for these beams. Figure 24 (a) presented the ultimate resistance of beams having Sections (C1). The effect of changing beam span on the ultimate

resistance is ignorable for those beams. For beams of Section (D1), Figure 24 (b) shows that increasing the beam span led to an increase in the ultimate resistance of these beams. It can be concluded that the effect of beam span variation has minor effect on increasing the ultimate resistance of prestressed composite beams compared to corresponding non-prestressed composite beams. The beam resistance is governed by the cross sectional capacity not the overall beam capacity. This may be attributed to the high resistance of composite beams to lateral buckling due to the presence of wide concrete deck in compression zone. Therefore, the ultimate resistance is affected by changing geometry of the cross section rather than changing the beam span.

7.3 Effect of Concrete Deck Thickness to Width Ratio

The effect of changing the concrete deck thickness to width ratio (h_c/B_c) is discussed for three types of tendon profiles. General view of results is presented, based on statistical data. In addition, a thorough discussion for the behavior of beams of Sections (A1) and (B1) is presented in the next subsections and the results are shown in Figures (25-30).

7.3.1 Straight tendon profile above tension flange (SA)

The maximum, minimum, and average percentages of increase in the ultimate resistance are shown in Figure 25.It can be seen from the figure that the percentage of increase in the ultimate resistance, due to prestressing, slightly increased by increasing concrete deck thickness to width ratio. Figure 26 gives better understanding of the effect of changing concrete deck thickness to width ratio in the presence of prestressing applied on composite beams. The ultimate moment (M_u) is considered for beams having aforementioned standard values. The ultimate moment of the non-prestressed composite beams (M_{uo}) is considered for corresponding beam with concrete deck thickness to width ratio ($h_c/B_c = 0.10$). Figures26 (a) and (b) show the results for Section (A1). It can be seen from the figures that the ultimate moment ratio increased by increasing the concrete deck thickness to width ratio for beams under concentrated and distributed loads. The ultimate moment ratios of beams of Section (B1) are presented in Figures 26 (c) and 26 (d). There is a direct relationship between ultimate moment and concrete deck thickness to width ratio.

7.3.2 Straight tendon profile below tension flange (SB)

Beams prestressed by straight tendon below bottom flange are investigated in this section. The percentage of increase in resistance is shown in Figure 27.It can be seen from the figure that the rate of increase in ultimate resistance due to prestressing increased by increasing the concrete deck thickness to width ratio. To thoroughly investigate the behavior, results of beams having Section (A1) are presented in Figures 28 (a) and (b). The ultimate resistance increases by increasing concrete deck thickness to width ratio. In Figures28 (c) and (d), results of prestressed composite beams of Section (B1) are presented. Clear direct relationship between concrete deck thickness to width ratio and ultimate moment ratio was also observed.

Accepted manuscript doi:
10.1680/jstbu.17.00172

7.3.3 Draped tendon profile (DR)

Figures 29 shows the maximum, minimum, and average values of percentage of increase in resistance. A notable increase was observed in the ultimate resistance due to prestressing by a draped tendon as the concrete deck thickness to width ratio increases. Figures 30 (a) and (b) presents the relation between ultimate moment ratio and concrete deck thickness to width ratio for beams of Section (A1). It can be seen from these figures that the ultimate moment ratio increased by increasing concrete deck thickness to width ratio, generally, for beams under concentrated and distributed loads. Figures 30 (c) and (d) showed direct relationship between ultimate resistance and concrete deck thickness to width ratio for prestressed composite beams of Section (B1).

It can be observed from the above that there is a direct relationship between ultimate resistance and concrete deck thickness to width ratio, as the ultimate resistance increased by increasing (h_c/B_c). This may be attributed to the increase in total section depth and the more uniform distribution of compressive stresses on concrete deck width, which increased by increasing (h_c/B_c).This is in agreement with Ibrahim et al [12] who observed the same when they stated that the strength of composite beams are increased by increasing the ratio of the depth to width of concrete slab, with keeping the total area of concrete slab constant.

8. Conclusion

A parametric study is performed for 2160 models using finite element analysis. The adopted modeling procedure is verified against two experimental tests on prestressed composite T-shaped beams of previous experimental work. Finite element results for three geometric parameters are presented and discussed. Some of the studied parameters are new such as the effect of beam span. The other parameters were investigated by previous researches with limited ranges. The investigated range of parameters in this study is wider than the range investigated by preceding researches in literature. The following conclusions can be drawn as follows:

1. It was found that there is a good agreement between the finite element results of the model used in the present study and the published experimental results. This was indicated by the very close agreement between the load-deflection relationships and the ultimate loads predicted by the finite element model and those of the experimental results. This insures the reliability and accuracy of the adopted model in predicting and analyzing the behavior of externally prestressed composite beams.
2. The tension flange area (bottom) to the compression flange area (top) ratio (A_{fb}/A_{ft}) is the most effective geometrical parameter on the prestressed beam ultimate resistance. It is worth mentioning that the total area of the two flanges is constant in all cases; i.e., the cross section area is constant for each group of sections in this investigation.

3. Increasing the (A_{fb}/A_{ft}) ratio led to an increase of the ultimate resistance of the beam. It was found that increasing the (A_{fb}/A_{ft}) ratio from 1 to 3 resulted in increasing the additional resistance of the beam due to prestressing from 15.4% to 46.1%. This is applicable for the three studied cable profiles and for beams under concentrated and distributed loads.
4. Variation of the beam resistance with span has no particular trend. This is not usual in the case of non-composite steel beams. In case of composite beams, the presence of concrete slab prevented the lateral-torsional buckling and accordingly minimized the effect of the span.
5. Increasing the slab thickness to width ratio resulted in enhancing the average increase in beam strength from 13.5% to 19.9%. This conclusion is applicable in all tendon profiles, all steel geometries, and all load cases studied in this research. The actual stress distribution across the width of concrete slab was implemented since the effect of the shear lag was considered by finite element analysis inclusively.
6. The current study shows that straight tendon profiles (SA and SB) are more appropriate for beams under distributed loads, while draped tendon profile is more convenient for beams under concentrated loads. Straight tendon profile below tension flange (SB) is slightly more efficient than straight tendon profile above tension flange (SA), the range of increase in ultimate resistance of beams with (SB) profile approximately from 3% and up to 7%.

Accepted manuscript doi:
10.1680/jstbu.17.00172

References

1. Lorenc, W., and Kubica, E., 2006, “Behavior of composite beams prestressed with external tendons: Experimental study”, J. of Constructional Steel Research, Vol. 62, pp.1353–1366.
2. Chen, S. and Gu, P., 2005, “Load carrying capacity of composite beams prestressed with external tendons under positive moment”, J. of Constructional Steel Research, Vol. 61, pp. 515–530.
3. Dall'Asta, A., Ragni, A., and Zona, A., 2007, “Simplified Method for Failure Analysis of Concrete Beams Prestressed with External Tendons”, J. of Structural Engineering, ASCE, Vol. 133, No. 1, pp. 121-131.
4. Nie J., Cai C., Zhou T.,and Li Y., 2007, "Experimental and Analytical Study of Prestressed Steel-Concrete Composite Beams Considering Slip Effect "ASCE, J. of Structural Engineering, Vol. 133, pp. 530-540.
5. Zona, A., Ragni, L. and Dall'Asta, A., 2009, “Simplified method for the analysis of externally prestressed steel-concrete composite beams”, J. of Const. Steel Research, Vol. 65, pp. 308-313.
6. Angomas, F. B., 2009, “Behavior of prestressed concrete bridge girders”, Master of science thesis submitted to Utah state university.
7. AASHTO LRFD Bridge Construction Specifications, Second Edition (2004), by the American Association of State Highway and Transportation Officials, 2006.
8. Dall'Asta, A. and Zona, A., 2005, “Finite element model for externally prestressed composite beams with deformable connection”, J. of Structural Engineering, ASCE, Vol. 131, No. 5, pp. 706-714.
9. Choi D., Kim Y., and Yoo H., 2008 "External Post-tensioning of Composite Bridges by a Rating Equation Considering the Increment of a Tendon Force Due to Live Loads" Steel Structures, Vol. 8, pp. 109-118.
10. Dabaon M., Sakr M. A., and Kharoub O., 2005, " Ultimate Behavior of Externally Prestressed Composite Beams with Partial Shear Connection" Department of Structural Engineering, Ain Shams University, Egypt.
11. El-Zohairy A. and Salim H., 2017, “Parametric study for post-tensioned composite beams with external tendons” Advances in Structural Engineering, Vol. 20, No. 10, pp. 1433–1450.
12. Chandramohanmouli K. and Kumar N. H., 2017, “Finite Element Modeling of Composite Steel-Concrete Beams with External Prestressing” International J. of Engineering Development and Research, Vol. 5, Issue 2, pp. 1889- 1907.
13. Ibrahim A. M., Mohaisen S. k., Ahmed Q. W., 2015, "Finite Element Modeling of Composite Steel-Concrete Beams with External Prestressing", International J. of Scientific & Engineering Research, Vol. 6, Issue 4, 15 pp.
14. Liban R. I. and Tayşi N., 2017, “Nonlinear Finite Element Analysis of Composite Cantilever Beam with External Prestressing”, International J. of Civil, Environmental, Structural, Construction, and Architectural Engineering Vol.11, No: 4, pp. 511-517.

15. Ibrahim A. M. and Salman W. D., 2015, "Parametric Study of Continuous Composite Steel-Concrete Beam with External Prestressing", Eng. & Tech. Journal, Vol.33, Part (A), No.3, 1261 ISSN 2229-5518, IJSER © 2015 http://www.ijser.org.
16. Lou T., and Xiang Y., 2010, "Numerical Analysis of Second-order Effects of Externally Prestressed Concrete Beams". Structural Engineering & Mechanics, Vol. 35, No. 5, pp. 631-643
17. Ibrahim A. M., Mohaisen S. k., Ahmed Q. W., 2015, "Parametric Study of Composite Steel-Concrete Beams with External Prestressing ", International J. of Scientific & Engineering Research, Vol. 6, Issue 4, pp. 1261-1269.
18. Bukka R. S., Shimpale P. M., and Lokhande R. M., 2016, "Non Linear Analysis of Composite Beam Slab Junction with Shear Connectors using ANSYS", Int. J. of Engg. Sci. Invention, Vol. 5, Issue 4, pp. 22-29.
19. ANSYS 14.0, Coupled Structural/Thermal Analysis, (ANSYS Tutorials). Copyright 2013 by University of Alberta.
20. Mahgoub E.M., Kamba, and Yanmin J., 2017, "Analysis of Behavior of Steel Box Girders Prestressed with External Tendons" The Open Civil Engineering Journal, Vol. 11.
21. Desayi P., and Krishnan, S., 1964, "Equation for the Stress-Strain Curve of Concrete", J. of the American Concrete Institute, Vol. 61, March, pp. 345- 350.
22. European Committee for Standardisation (CEB), Eurocode 2, 1993, "Design of Concrete Structures", Part 1.1: General Rules and Rules for Buildings, DD ENV 1993-1-1, EC2.
23. Chen, S., 2005, "Experimental study of prestressed steel–concrete composite beams with external tendons for negative moments", J. of Constructional Steel Research 61, pp. 1613–1630.
24. Chen, S., Wang, X. and Jia, Y., 2009, "A comparative study of continuous steel-concrete composite beams prestressed with external tendons: Experimental investigation", J. of Constructional Steel Research 65, pp. 1480-1489.
25. Kim, K.S., Lee, D.H, 2011, "Flexural behavior of prestressed composite beams with corrugated web: Part II. Experiment and verification", Composites: Part B 42, pp. 1617–1629
26. Lorenc, W., and Kubica, E., 2006, "Behavior of composite beams prestressed with external tendons: Experimental study", J. of Constructional Steel Research 62, pp.1353–1366.
27. Nie J., Cai C., Zhou T.,and Li Y., 2007, "Experimental and Analytical Study of Prestressed Steel-Concrete Composite Beams Considering Slip Effect "ASCE, J. of Structural Engineering 133, pp. 530-540.
28. Safan M., and Kohoutkova A., 2001, "Experiments with Externally Prestressed Continuous Composite Girders" .Acta Polytechnica 41, pp. 65-73.
29. Zong Z., Zheng Z., Fang Z., and Che. H., 2002, "Experimental Study of External Prestressed Steel-Concrete Composite Continuous Beams". China J. of Highway and Trans. 15, pp. 44-49.
30. Saadatmanesh H., AlbrechtP, and Ayyub B., 1989,'' Experimental Study of Prestressed Composite Beams" ASCE, J. of Structural Engineering, Vol. 115, pp. 2348-2363.

31. Ayyub B., Sohn Y., and Saadatmanesh H., 1990,“Prestressed Composite Girders under Positive Moment". ASCE, J. of Structural Engineering, Vol. 116, pp. 2931-2951.

32. Shiming C., Yuanlin J. “Numerical investigation of inelastic buckling of steel-concrete composite beams prestressed with external tendons”. Thin-Walled Structures, Volume 48, Issue, 2010,pp.233-242.

33. Tiejiong L., Sergio M.R. L., Adelino V. L. “Numerical modeling of externally prestressed steel-concrete composite beams”. Journal of Constructional Steel Research, Volume 121, 2016, pp. 229-236.

Accepted manuscript doi:
10.1680/jstbu.17.00172

Table 1 Material properties of samples for verification purposes

Sample Beam	f_{pe}(MPa)	f_{py} (MPa)	f_c' (MPa)	f_y(Flange) (MPa)	f_y (Web) (MPa)	Reference
VB1	544	910	33.4	367	367	Saadatmanesh et al. [30]
VB2	1046	1620	40.0	411.6	411.6	Ayyub et al. [31]

Table 2 Geometrical properties of sample beams for verification purposes

Sample Beam	h_s (mm)	h_w (mm)	t_w(mm)	b_t & b_b (mm)	t_t & t_b (mm)	B_c (mm)	h_c (mm)	h_e (mm)
VB1	352	333	6.8	172	9.5	915	76	-57
VB2	371	352	6.8	172	9.5	1070	90	30

h_e: *positive sign for tendon above flange and negative sign for tendon below flange.*

Table 3 Steel cross-sections dimensions.

Section	h_w (mm)	t_w (mm)	b_b (mm)	t_b (mm)	b_t (mm)	t_t (mm)	A_{fb} /A_{ft}
A1	500	8	200	10	200	10	1
B1	500	8	300	16	300	16	
C1	750	10	200	10	200	10	
D1	750	10	300	16	300	16	
A2	500	8	222	12	167	8	2
B2	500	8	320	20	229	14	
C2	750	10	222	12	167	8	
D2	750	10	320	20	229	14	
A3	500	8	250	12	143	7	3
B3	500	8	360	20	200	12	
C3	750	10	250	12	143	7	
D3	750	10	360	20	200	12	

Table 4 Material properties of prestressed composite beams

Material	Parameter	Symbol	Value
Concrete	Compressive Strength (MPa)	F_c'	30
	Modulus of elasticity (MPa)	E_c	25743
Steel beam, steel plates, and reinforcement, and studs	Yield stress (MPa)	F_y	360
	Ultimate Strength (MPa)	F_u	520
	Modulus of elasticity (MPa)	Es	210000
Prestressing tendon	Yield stress (MPa)	F_{py}	1680
	Ultimate Strength (MPa)	F_{pu}	1860
	Modulus of elasticity (MPa)	E_{ps}	200000

E_c: *As per (ACI 318).*

Figure 1 Boundary conditions of beam. (a) Hinged support condition (b) Roller support condition

Figure 2 Stress-strain relationships used in modeling the studied beams. (a) Simplified compressive uniaxial stress-strain curve for concrete [21]. (b) Alternative bilinear stress-strain relationship for steel [22].

Figure 3 Typical cross-section of externally prestressed composite beam.

Figure 4 Details, deformed shapes, and load-deflection results of Beam VB1 [30]. (a) Details of the first sample studied beam. (All dimensions are in mm) (b) Load-deflection curve. (c) Initial camber (cm). (d) At ultimate state (cm).

Figure 5 Details, deformed shapes, and load-deflection results of Beam VB2 [31]. (a) Details of the second sample studied beam. (All dimensions are in mm) (b) Load-deflection curve. (c) Initial camber (cm). (d) At ultimate load (cm).

Figure 6 Tendons profiles. (a) First tendon profile (SA) (b) Second tendon profile (SB) (c) Third tendon profile (DR)

Figure 7 Effect of steel flange area ratio on the ultimate resistance of beams (SA). (a) Under concentrated loads (b) Under distributed loads

Figure 8 Effect of steel flange area ratio on the ultimate resistance of PCB (SA) (a) Under concentrated loads (b) Under distributed loads (c) Under concentrated loads (d) Under distributed loads

Figure 9 Effect of steel flange area ratio on the ultimate resistance of beams (SB). (a) Under concentrated loads (b) Under distributed loads

Figure 10 Effect of flange area ratio on the ultimate resistance of PCB (SB) Sec. (B). (a) Under concentrated loads (b) Under distributed loads (c) Under concentrated loads (d) Under distributed loads

Figure 11 Effect of steel flange area ratio on the ultimate resistance of beams (DR). (a) Under concentrated loads (b) under distributed loads

Figure 12 Effect of flange area ratio on the ultimate resistance of PCB (DR) Sec. (B). (a) Under concentrated loads (b) Under distributed loads (c) Under concentrated loads (d) Under distributed loads

Figure 13 Effect of beam span on the ultimate resistance of beams (SA) Sec. (A&B). (a) Under concentrated loads (b) Under distributed loads

Figure 14 Effect of beam span on the ultimate resistance of beams (SA) Sec. (C&D). (a) Under concentrated loads (b) Under distributed loads

Figure 15 Effect of beam span on the ultimate resistance of PCB (SA) (h_w = 500m). (a) Sec. (A1) (b) Sec. (B1)

Figure 16 Effect of beam span on the ultimate resistance of PCB (SA) (h_w = 750m). (a) Sec. (C1)) (b) Sec. (D1))

Figure 17 Effect of beam span on the ultimate resistance of beams (SB) Sec. (A&B). a) Under concentrated loads b) Under distributed loads

Figure 18 Effect of beam span on the ultimate resistance of beams (SB) Sec. (C&D). a) Under concentrated loads b) Under distributed loads

Figure 19 Effect of beam span on the ultimate resistance of PCB (SB) (h_w = 500m). (a) Sec. (A1)) (b) Sec. (B1))

Figure 20 Effect of beam span on the ultimate resistance of PCB (SB) (h_w = 750m). (a) Sec. (C1) (b) Sec. (D1)

Figure 21 Effect of beam span on the ultimate resistance of beams (DR) Sec. (A&B). (a) Under concentrated loads (b) Under distributed loads

Figure 22 Effect of beam span on the ultimate resistance of beams (DR) Sec. (C&D). (a) Under concentrated loads (b) Under distributed loads

Figure 23 Effect of beam span on the ultimate resistance of PCB (DR) Sec. (A1&B1). (a) Sec. (A1) (b) Sec. (B1)

Figure 24 Effect of beam span on the ultimate resistance of PCB (DR) Sec. (C1&D1). (a) Sec. (C1) (b) Sec. (D1)

Figure 25 Effect of concrete deck thickness to width ratio on the ultimate resistance of beams (a) Under concentrated loads (b) Under distributed loads

Figure 26 Effect of concrete deck thickness to width ratio on the ultimate resistance of PCB (SA) (a) Under concentrated loads (b) Under distributed loads (c) Under concentrated loads (d) Under distributed loads

Figure 27 Effect of concrete deck thickness to width ratio on the ultimate resistance of beams (SB). (a) Under concentrated loads (b) Under distributed loads

Figure 28 Effect of concrete deck thickness to width ratio on the ultimate resistance of PCB (SB) (a) Under concentrated loads (b) Under distributed loads (c) Under concentrated loads (d) Under distributed loads

Figure 29 Effect of concrete deck thickness to width ratio on the ultimate resistance of beams (DR). (a) Under concentrated loads (b) Under distributed loads

Figure 30 Effect of concrete deck thickness to width ratio on the ultimate resistance of PCB (DR) (a) Under concentrated loads (b) Under distributed loads (c) Under concentrated loads (d) Under distributed loads

Accepted manuscript doi:
10.1680/jstbu.17.00172

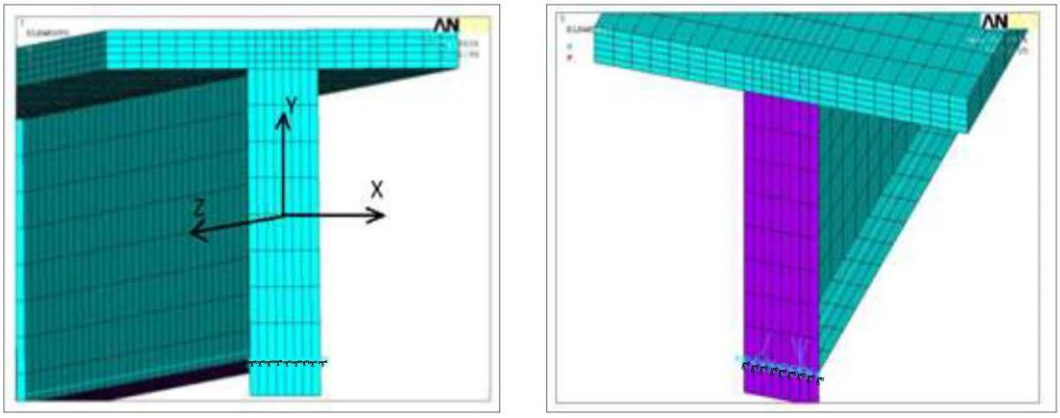

(a) Hinged support condition (b) Roller support condition

Figure 1 Boundary conditions of beam.

Accepted manuscript doi:
10.1680/jstbu.17.00172

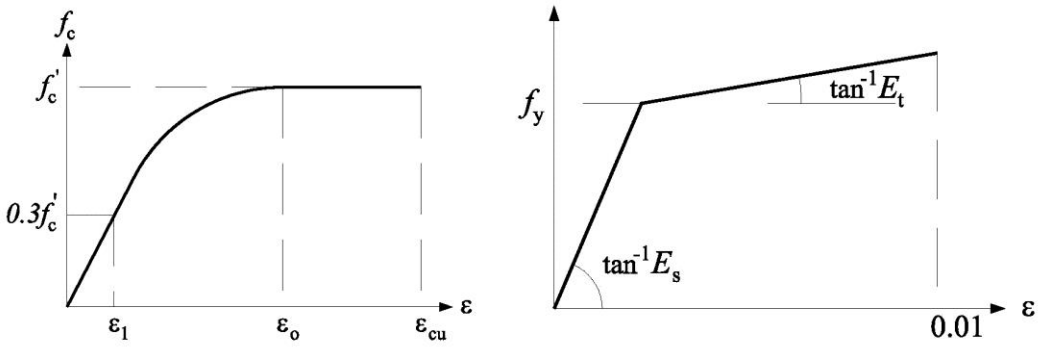

(a) Simplified compressive uniaxial stress-strain curve for concrete [21].

(b) Alternative bilinear stress-strain relationship for steel [22].

Figure 2 Stress-strain relationships used in modeling the studied beams.

Accepted manuscript doi:
10.1680/jstbu.17.00172

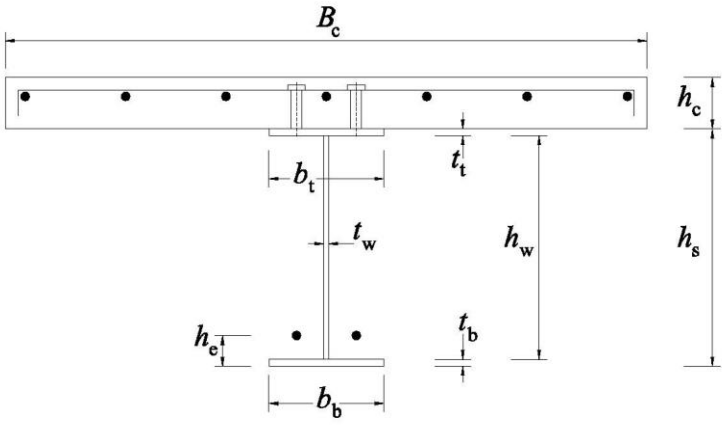

Figure 3 Typical cross-section of externally prestressed composite beam.

Accepted manuscript doi:
10.1680/jstbu.17.00172

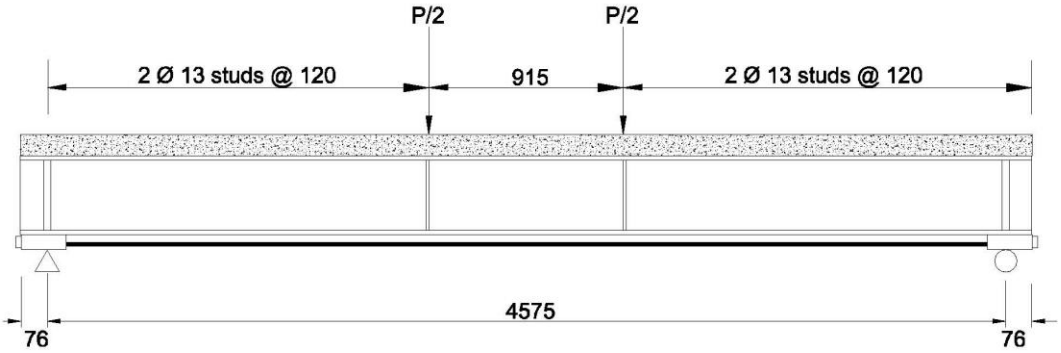

(a) Details of the first sample studied beam. (All dimensions are in mm)

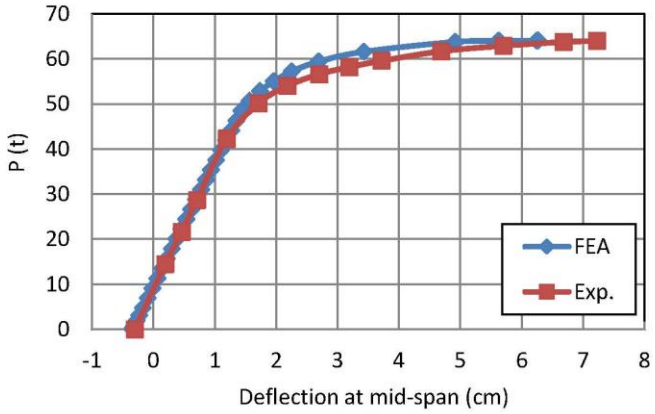

(b) Load-deflection curve.

Accepted manuscript doi:
10.1680/jstbu.17.00172

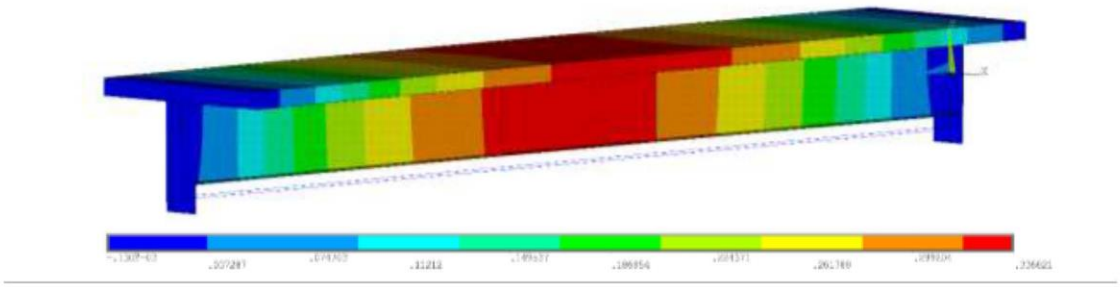

(c) Initial camber (cm).

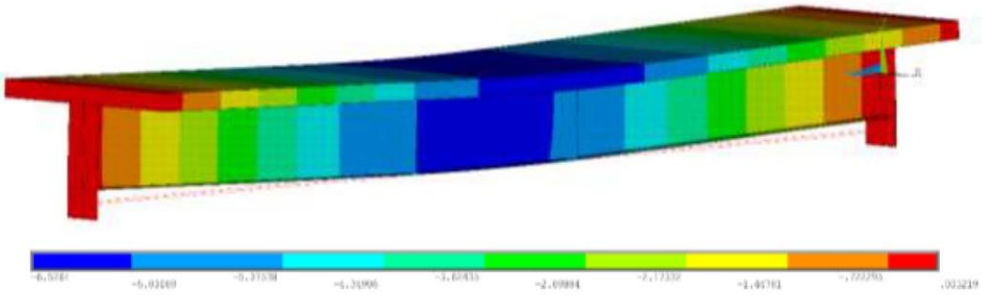

(d) At ultimate state (cm).

Figure 4 Details, deformed shapes, and load-deflection results of Beam VB1 [30].

Accepted manuscript doi:
10.1680/jstbu.17.00172

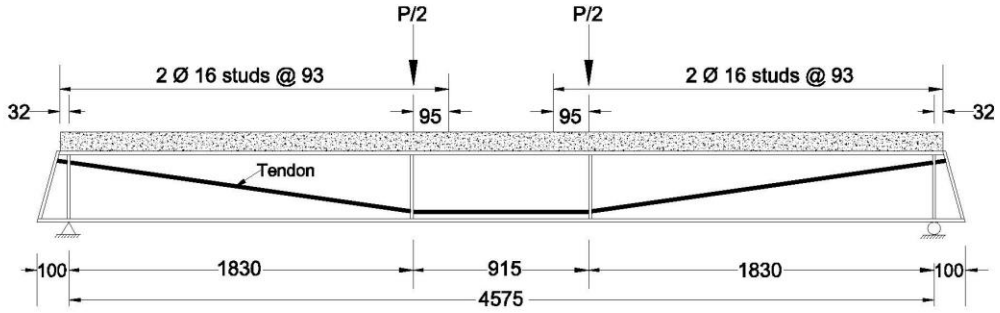

(a) Details of the second sample studied beam. (All dimensions are in mm)

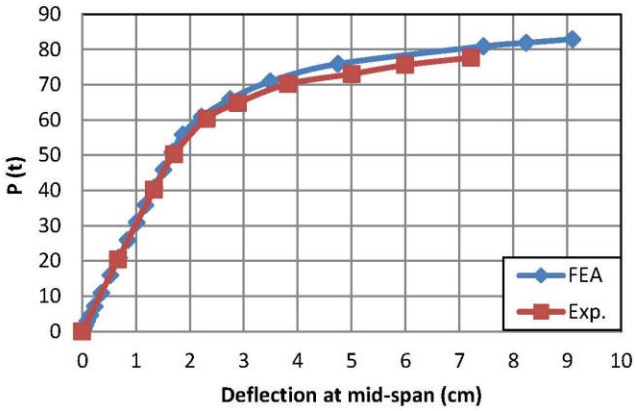

(c) Load-deflection curve.

Accepted manuscript doi:
10.1680/jstbu.17.00172

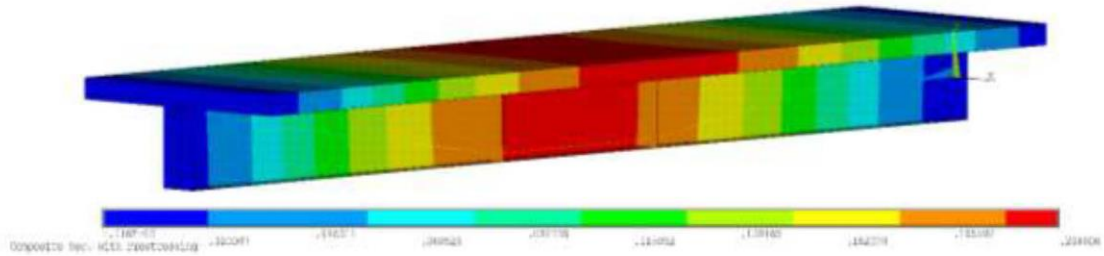

(c) Initial camber (cm).

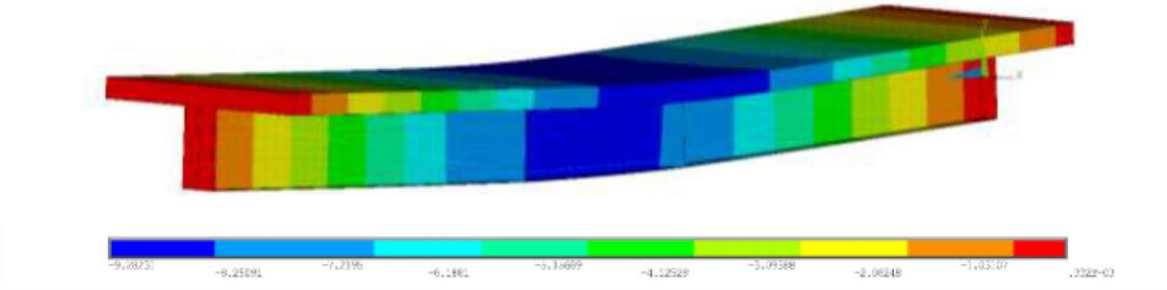

(d) At ultimate load (cm).

Figure 5 Details, deformed shapes, and load-deflection results of Beam VB2 [31].

Accepted manuscript doi:
10.1680/jstbu.17.00172

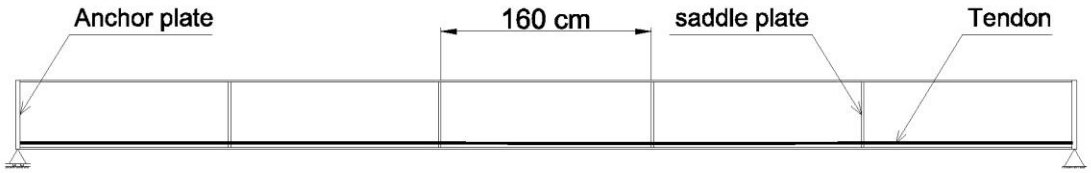

(a) First tendon profile (SA)

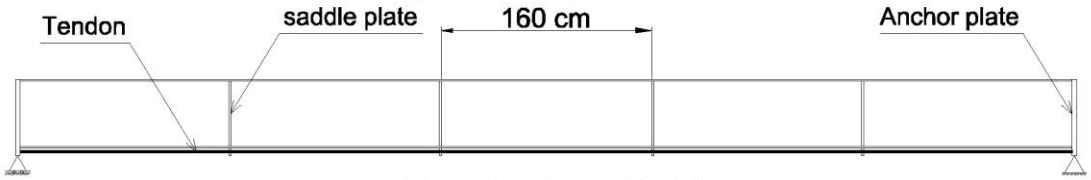

(b) Second tendon profile (SB)

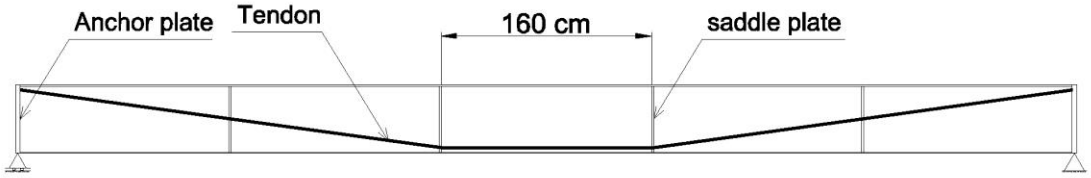

(c) Third tendon profile (DR)

Figure 6 Tendons profiles.

Accepted manuscript doi:
10.1680/jstbu.17.00172

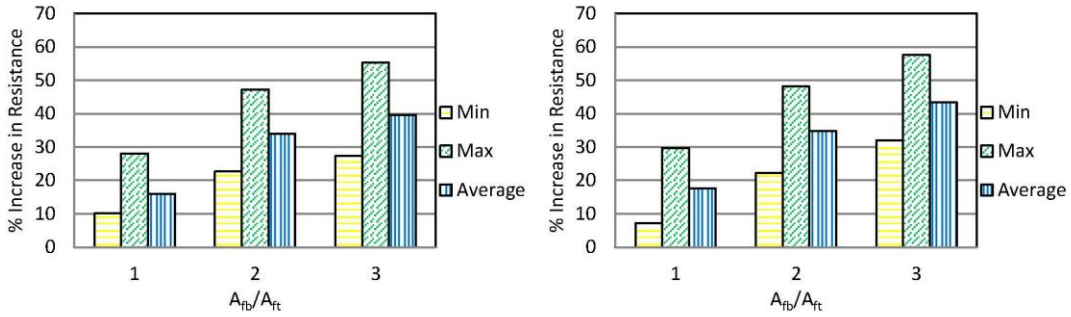

(a) Under concentrated loads (b) Under distributed loads

Figure 7 Effect of steel flange area ratio on the ultimate resistance of beams (SA).

Accepted manuscript doi:
10.1680/jstbu.17.00172

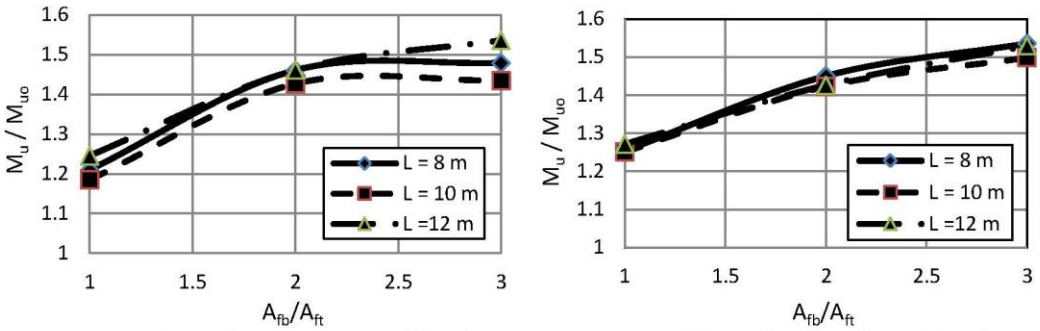

(a) Under concentrated loads (b) Under distributed loads

Section (A)

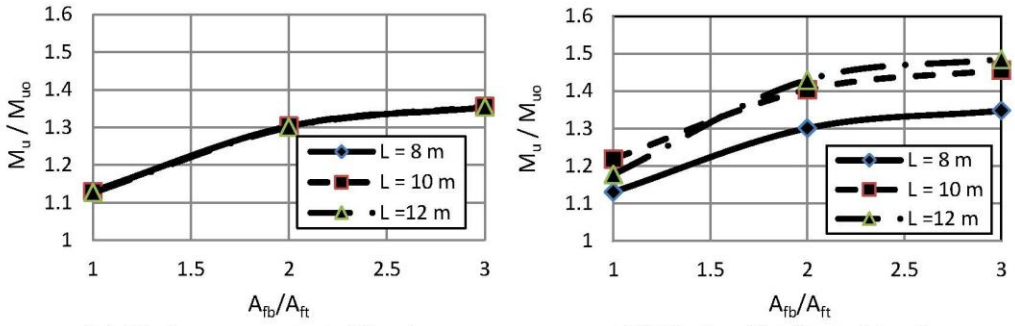

(c) Under concentrated loads (d) Under distributed loads

Section (B)

Figure 8 Effect of steel flange area ratio on the ultimate resistance of PCB (SA)

Accepted manuscript doi:
10.1680/jstbu.17.00172

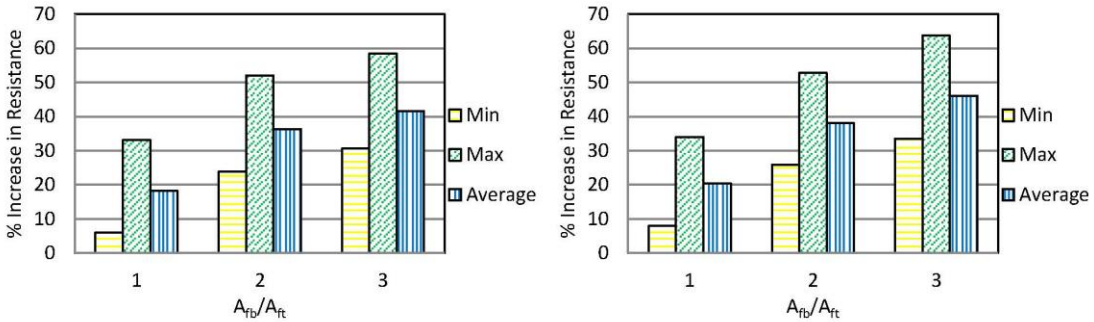

(a) Under concentrated loads (b) Under distributed loads

Figure 9 Effect of steel flange area ratio on the ultimate resistance of beams (SB).

Accepted manuscript doi:
10.1680/jstbu.17.00172

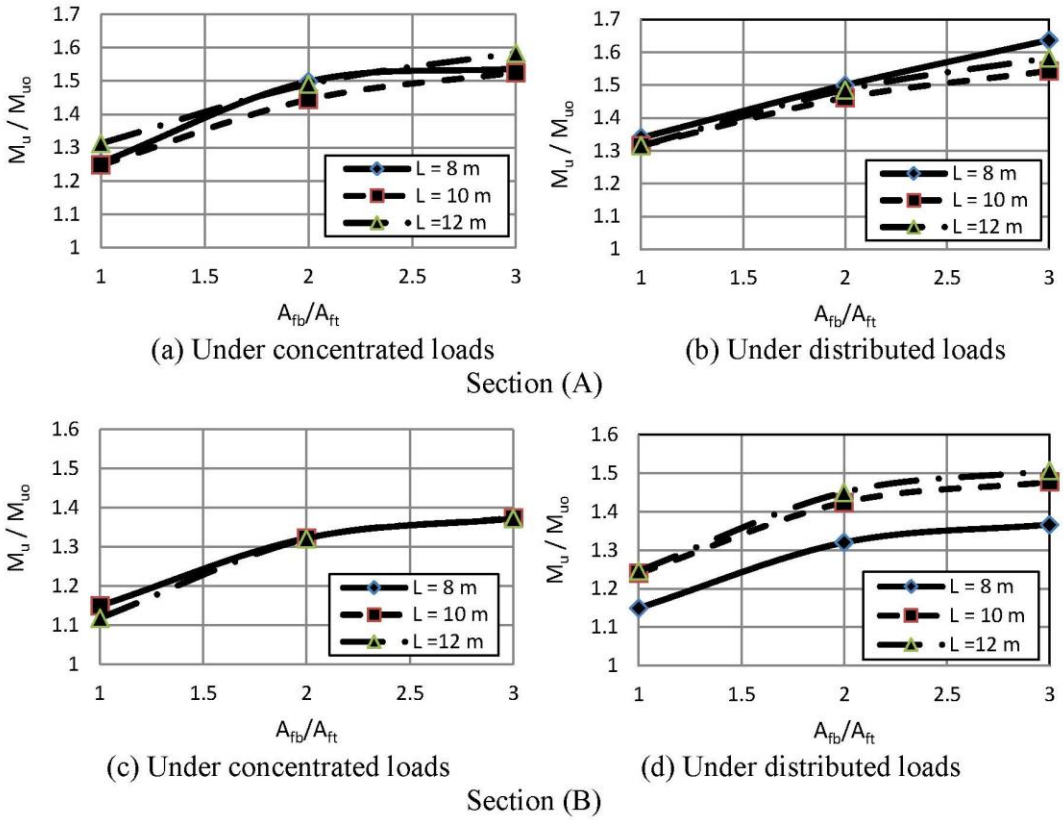

(a) Under concentrated loads (b) Under distributed loads

Section (A)

(c) Under concentrated loads (d) Under distributed loads

Section (B)

Figure 10 Effect of flange area ratio on the ultimate resistance of PCB (SB) Sec. (B).

Accepted manuscript doi:
10.1680/jstbu.17.00172

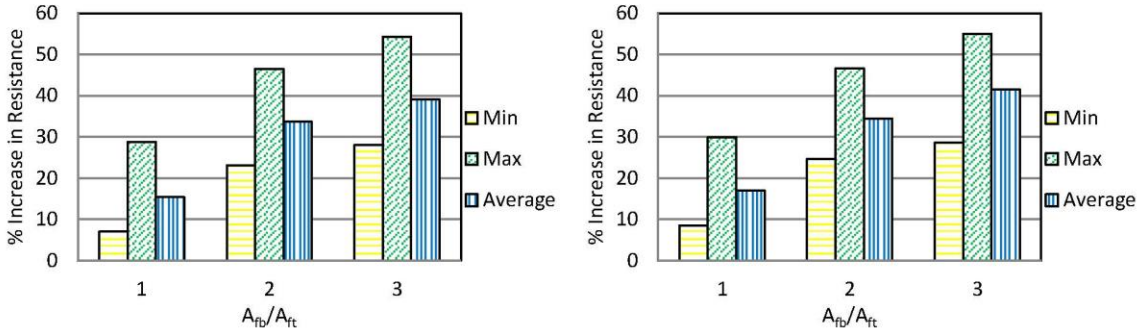

(a) Under concentrated loads (b) Under distributed loads

Figure 11 Effect of steel flange area ratio on the ultimate resistance of beams (DR).

Accepted manuscript doi:
10.1680/jstbu.17.00172

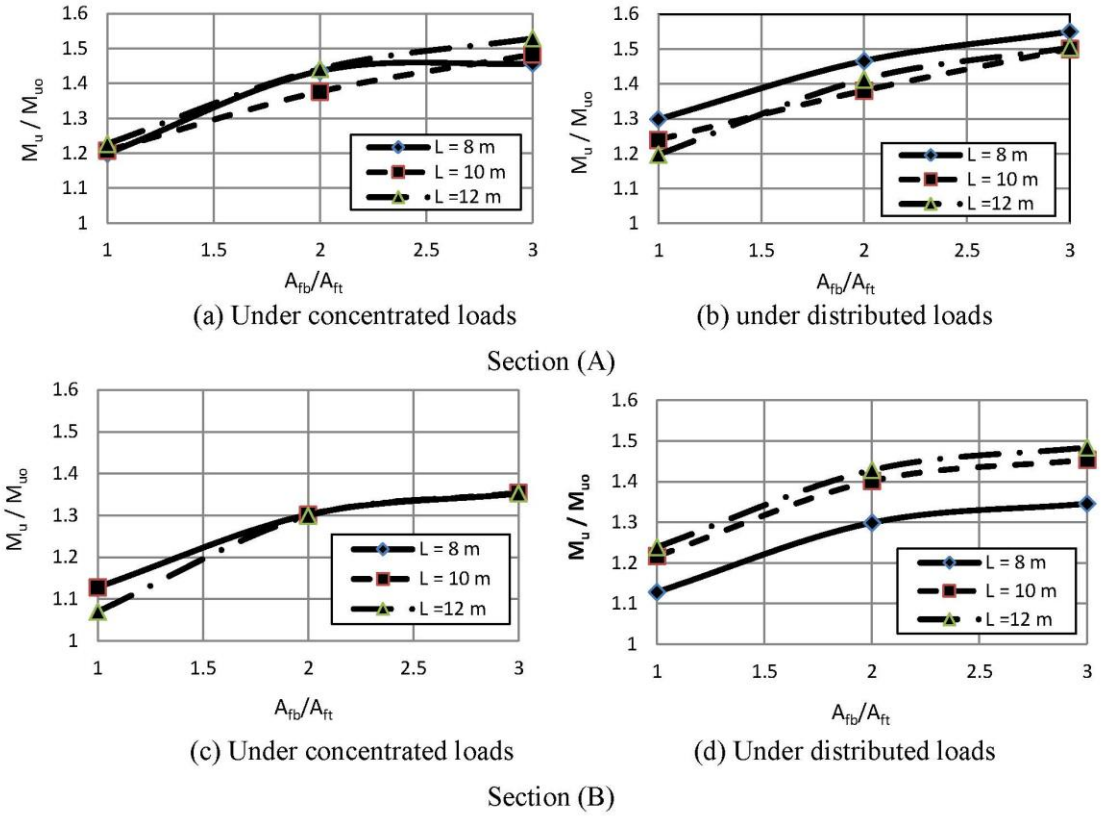

(a) Under concentrated loads (b) under distributed loads

Section (A)

(c) Under concentrated loads (d) Under distributed loads

Section (B)

Figure 12 Effect of flange area ratio on the ultimate resistance of PCB (DR) Sec. (B).

Accepted manuscript doi:
10.1680/jstbu.17.00172

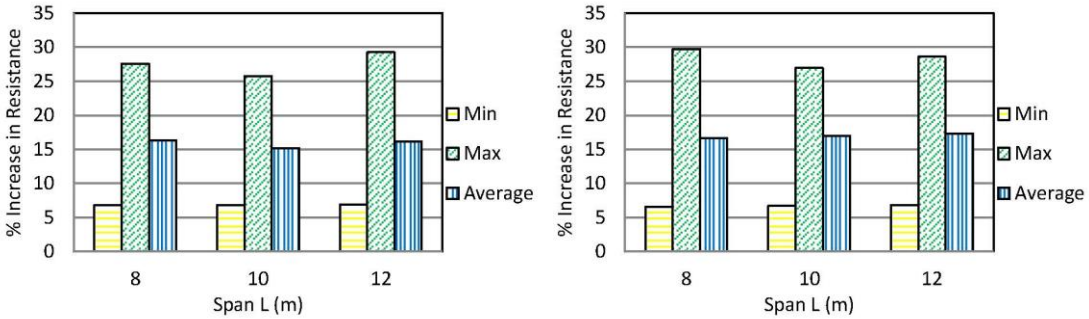

(a) Under concentrated loads (b) Under distributed loads

Figure 13 Effect of beam span on the ultimate resistance of beams (SA) Sec. (A & B).

Accepted manuscript doi:
10.1680/jstbu.17.00172

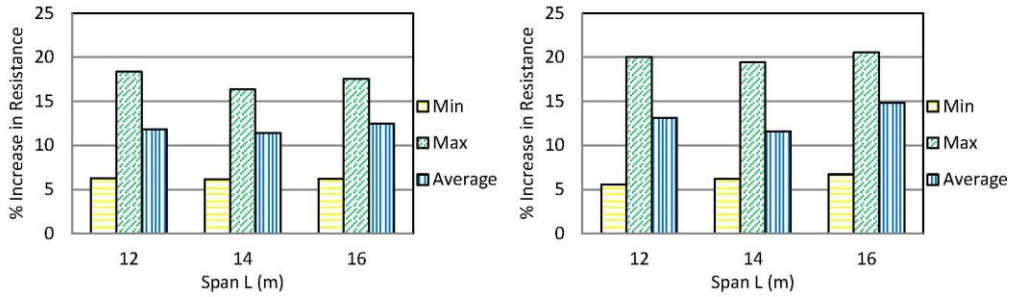

(a) Under concentrated loads (b) Under distributed loads

Figure 14 Effect of beam span on the ultimate resistance of beams (SA) Sec. (C & D).

Accepted manuscript doi:
10.1680/jstbu.17.00172

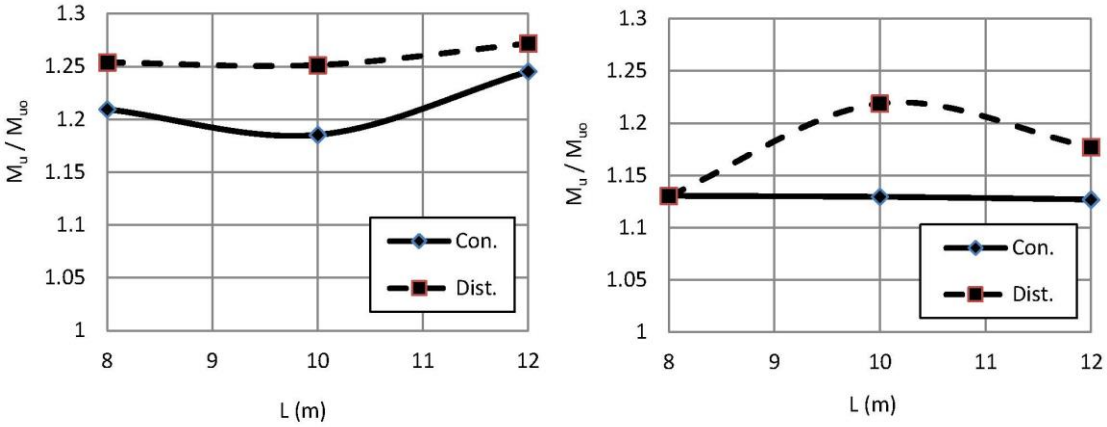

(a) Sec. (A1) (b) Sec. (B1)

Figure 15 Effect of beam span on the ultimate resistance of PCB (SA) (h_w = 500m).

Accepted manuscript doi:
10.1680/jstbu.17.00172

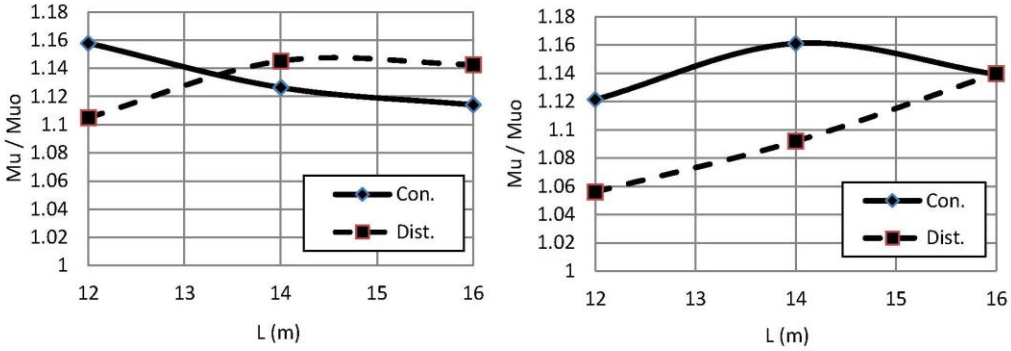

(a) Sec. (C1))

(b) Sec. (D1))

Figure 16 Effect of beam span on the ultimate resistance of PCB (SA) (h_w = 750m).

Accepted manuscript doi:
10.1680/jstbu.17.00172

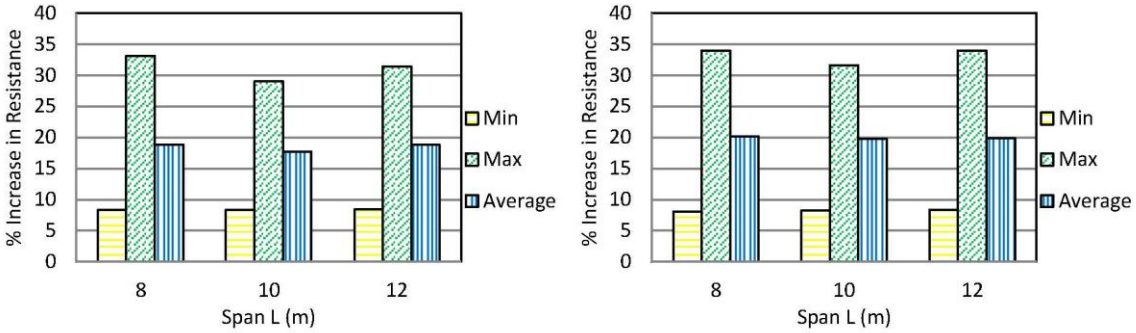

a) Under concentrated loads b) Under distributed loads

Figure 17 Effect of beam span on the ultimate resistance of beams (SB) Sec. (A & B).

Accepted manuscript doi:
10.1680/jstbu.17.00172

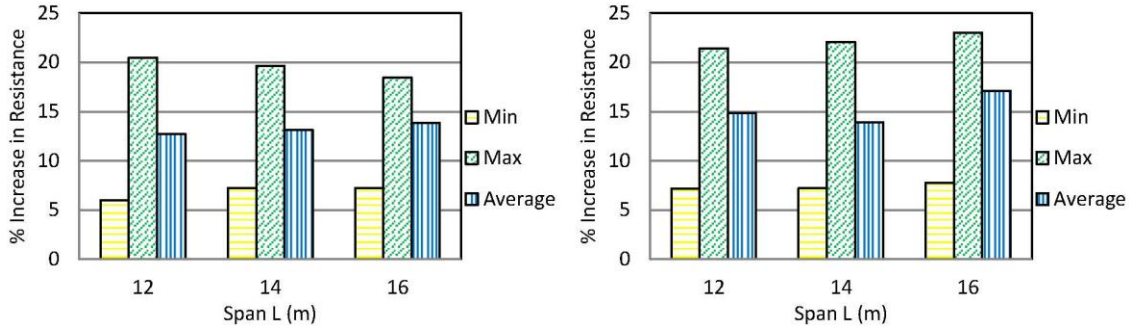

a) Under concentrated loads b) Under distributed loads

Figure 18 Effect of beam span on the ultimate resistance of beams (SB) Sec. (C & D).

Accepted manuscript doi:
10.1680/jstbu.17.00172

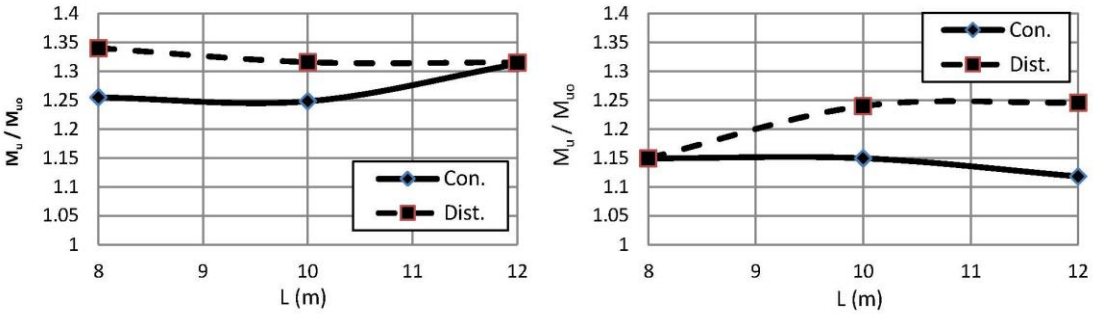

(a) Sec. (A1)) (b) Sec. (B1))

Figure 19 Effect of beam span on the ultimate resistance of PCB (SB) (h_w = 500m).

Accepted manuscript doi:
10.1680/jstbu.17.00172

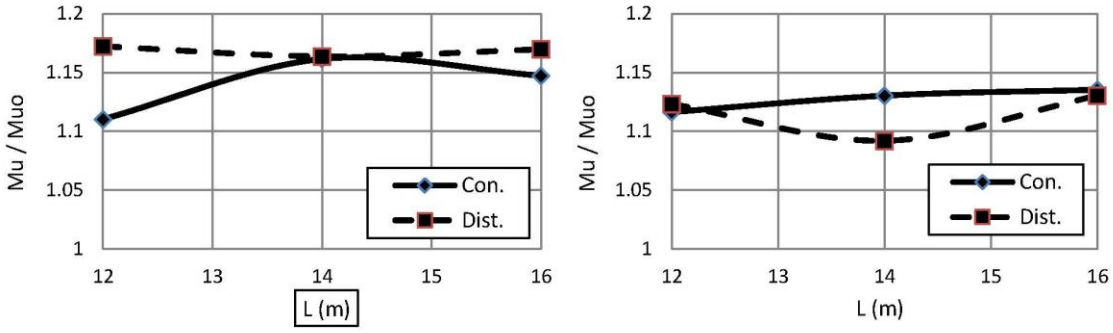

(a) Sec. (C1) (b) Sec. (D1)

Figure 20 Effect of beam span on the ultimate resistance of PCB (SB) (h_w = 750m).

Accepted manuscript doi:
10.1680/jstbu.17.00172

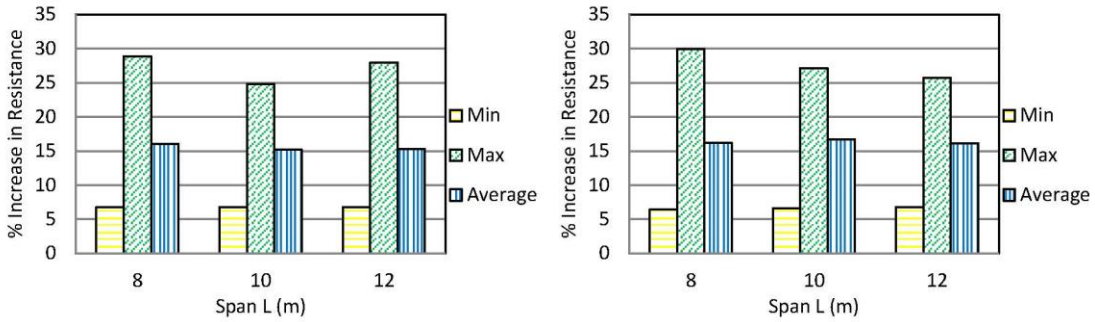

(a) Under concentrated loads (b) Under distributed loads

Figure 21 Effect of beam span on the ultimate resistance of beams (DR) Sec. (A&B).

Accepted manuscript doi:
10.1680/jstbu.17.00172

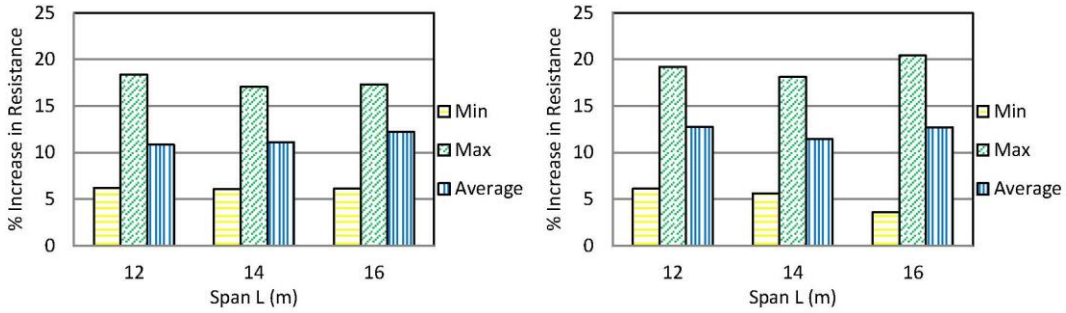

(a) Under concentrated loads (b) Under distributed loads

Figure 22 Effect of beam span on the ultimate resistance of beams (DR) Sec. (C&D).

Accepted manuscript doi:
10.1680/jstbu.17.00172

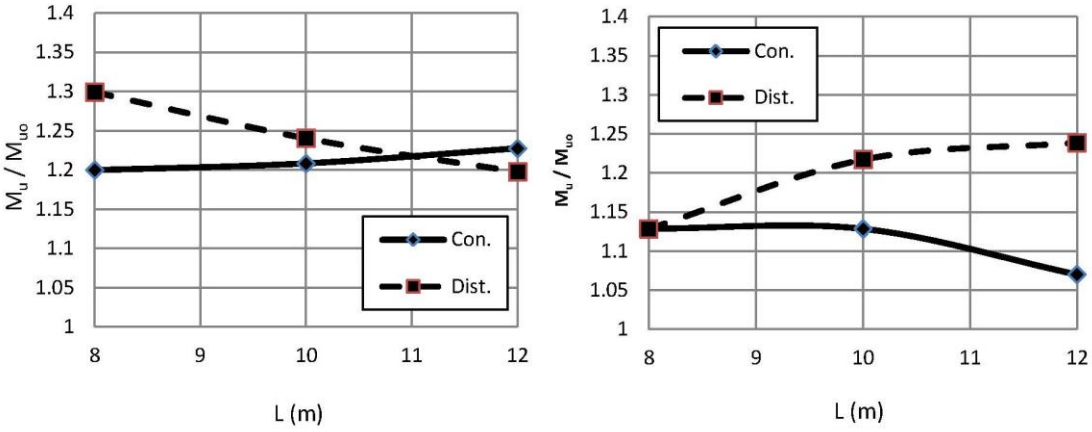

(a) Sec. (A1) (b) Sec. (B1)

Figure 23 Effect of beam span on the ultimate resistance of PCB (DR) Sec. (A1&B1).

Accepted manuscript doi:
10.1680/jstbu.17.00172

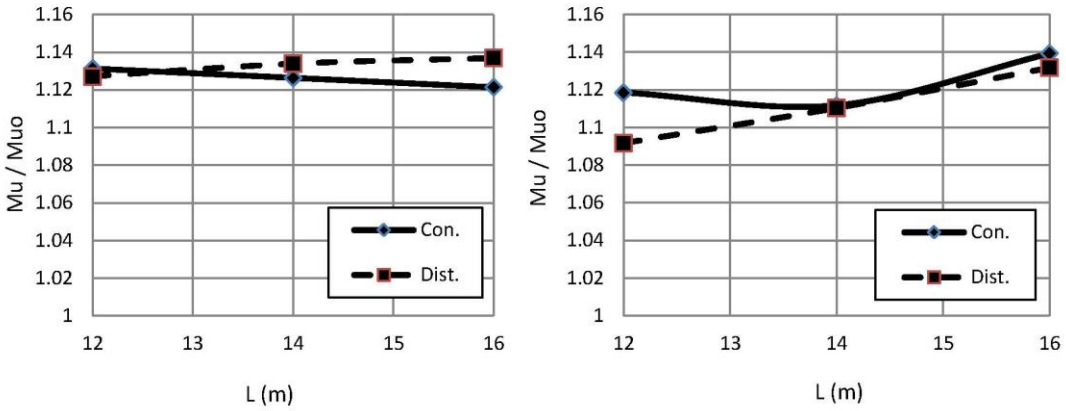

(a) Sec. (C1) (b) Sec. (D1)

Figure 24 Effect of beam span on the ultimate resistance of PCB (DR) Sec. (C1&D1).

Accepted manuscript doi:
10.1680/jstbu.17.00172

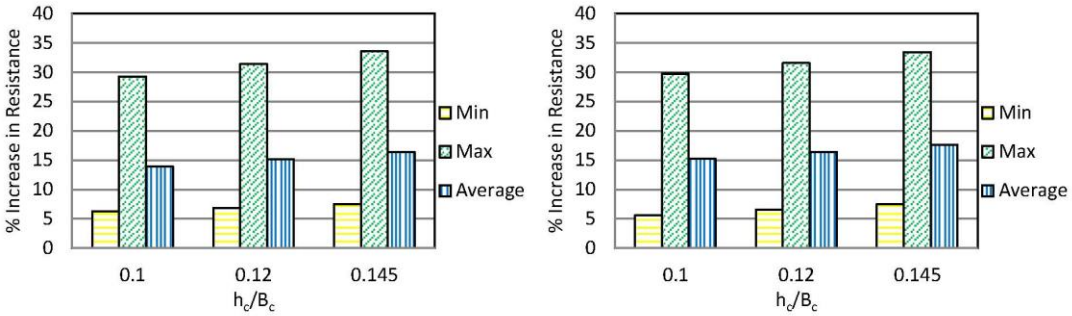

Figure 25 Effect of concrete deck thickness to width ratio on the ultimate resistance of beams

Accepted manuscript doi:
10.1680/jstbu.17.00172

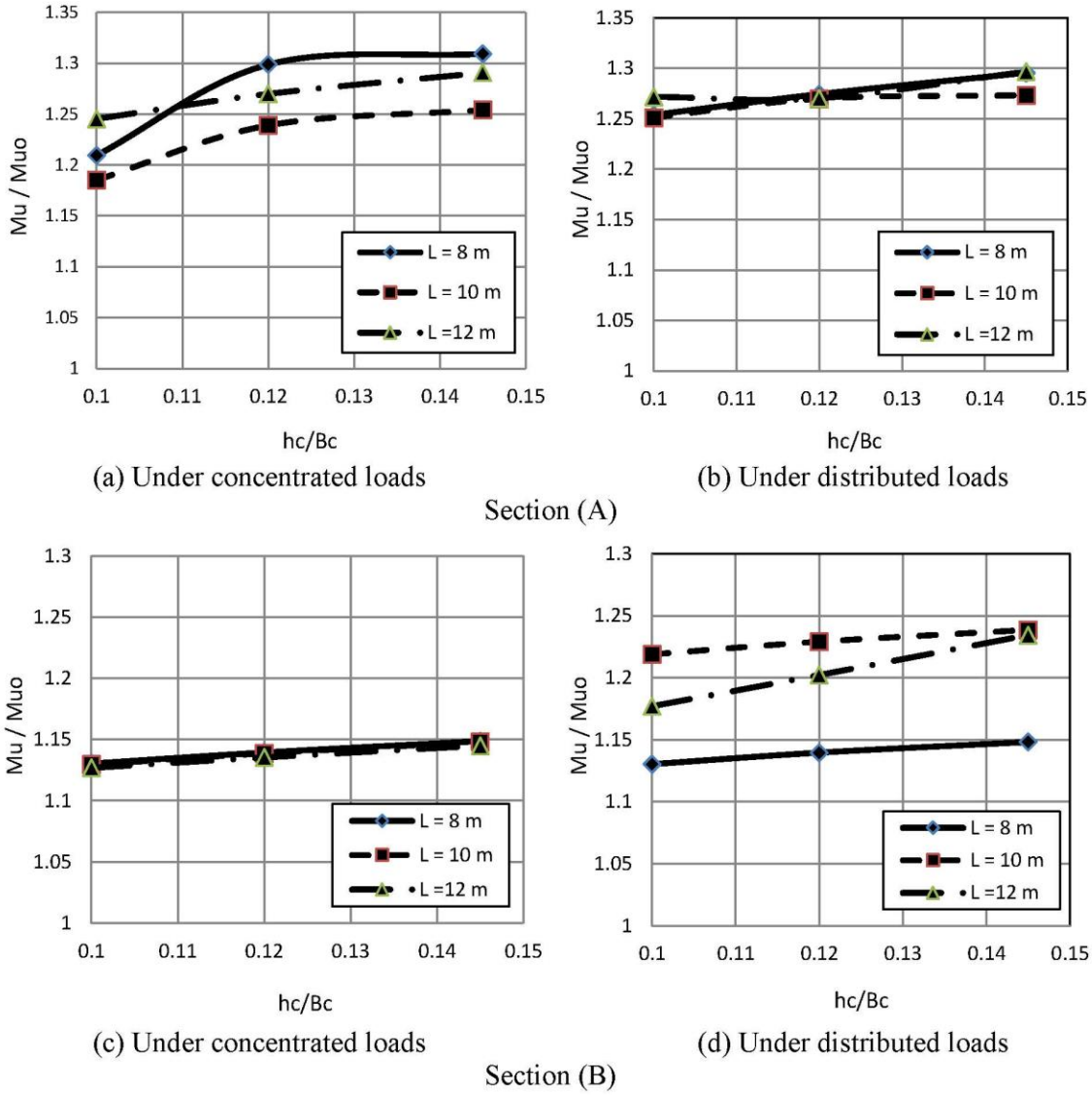

Figure 26 Effect of concrete deck thickness to width ratio on the ultimate resistance of PCB (SA)

Accepted manuscript doi:
10.1680/jstbu.17.00172

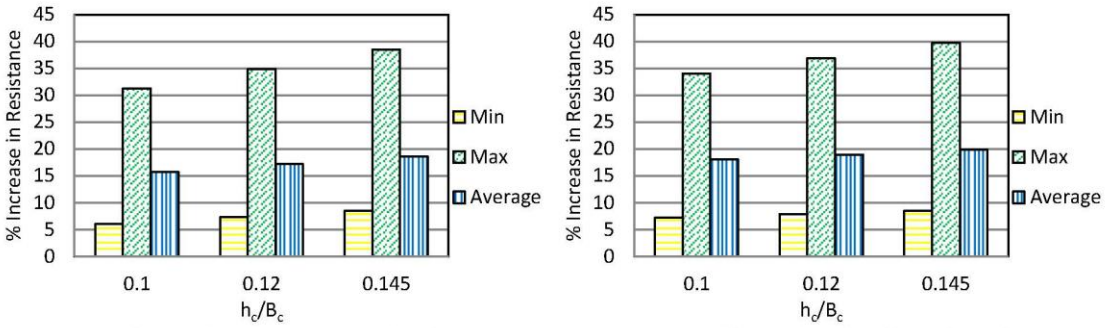

(a) Under concentrated loads (b) Under distributed loads

Figure 27 Effect of concrete deck thickness to width ratio on the ultimate resistance of beams (SB).

Accepted manuscript doi:
10.1680/jstbu.17.00172

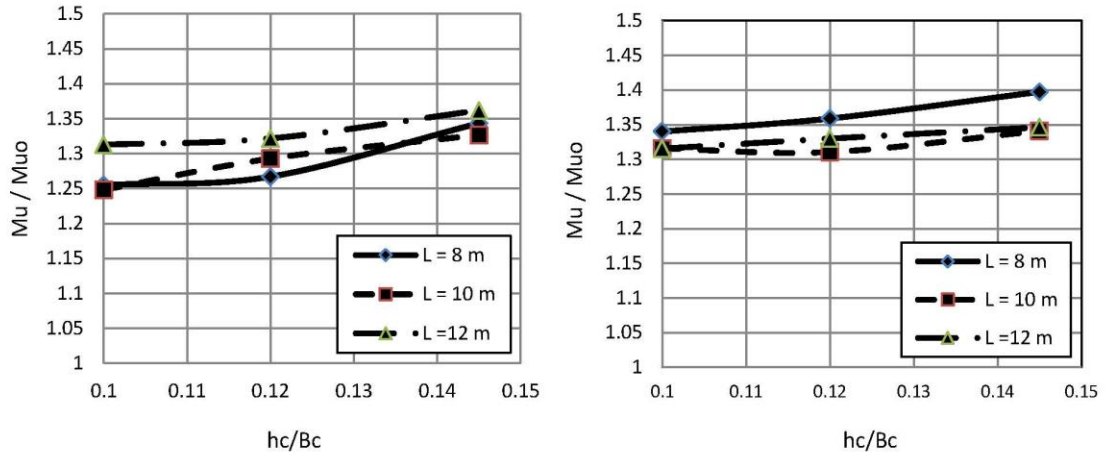

(a) Under concentrated loads (b) Under distributed loads

Section (A)

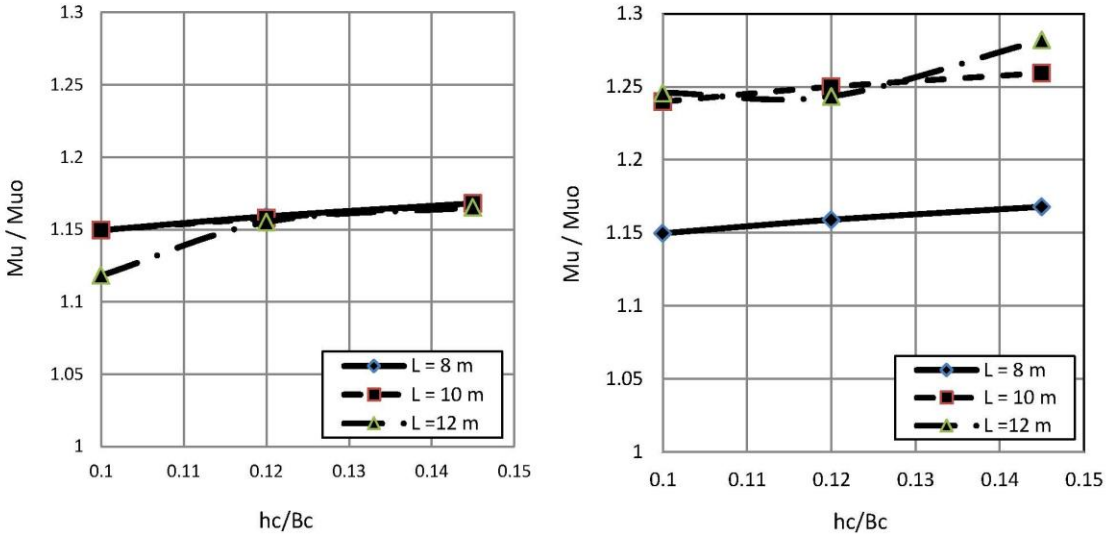

(c) Under concentrated loads (d) Under distributed loads

Section (B)

Figure 28 Effect of concrete deck thickness to width ratio on the ultimate resistance of PCB (SB)

Accepted manuscript doi:
10.1680/jstbu.17.00172

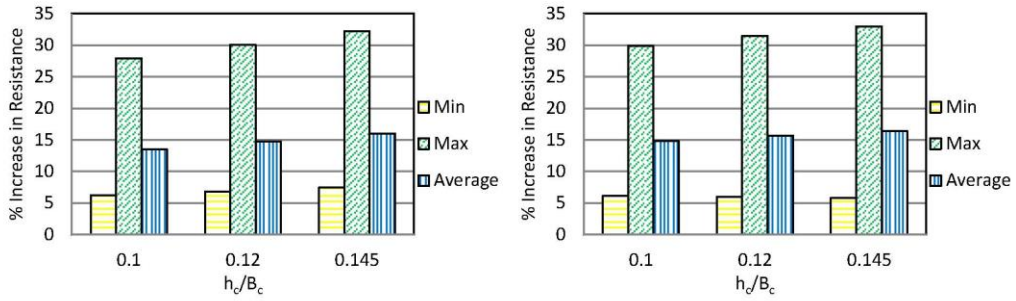

(a) Under concentrated loads (b) Under distributed loads

Figure 29 Effect of concrete deck thickness to width ratio on the ultimate resistance of beams (DR).

Accepted manuscript doi:
10.1680/jstbu.17.00172

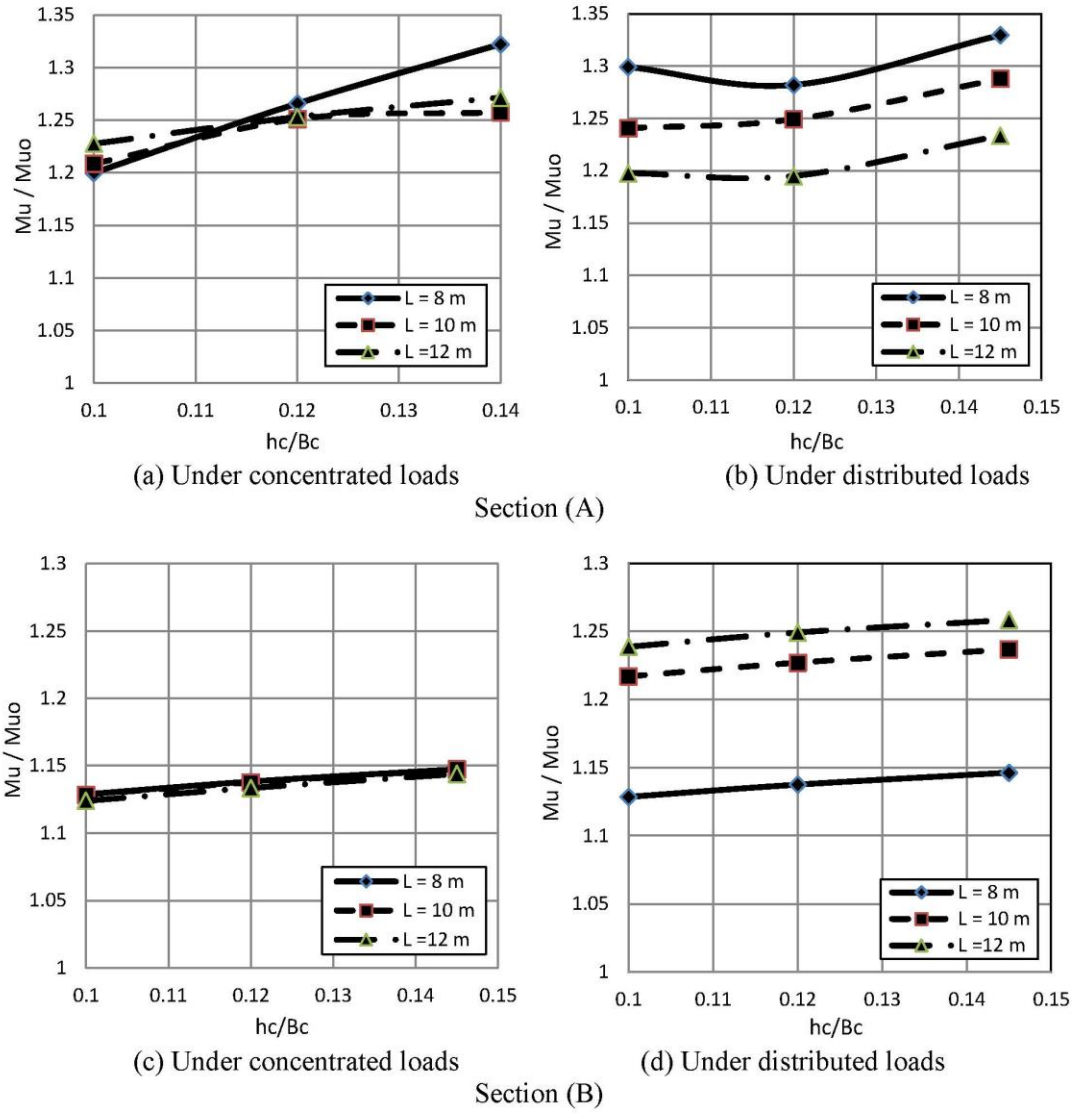

Figure 30 Effect of concrete deck thickness to width ratio on the ultimate resistance of PCB (DR)